Earth and Planetary Science Letters 565 (2021) 116965

Contents lists available at ScienceDirect

Earth and Planetary Science Letters

www.elsevier.com/locate/epsl

Zircon geochronology suggests a long-living and active magmatic system beneath the Ciomadul volcanic dome field (eastern-central Europe)

R. Lukács [a,*], L. Caricchi [b], A.K. Schmitt [c], O. Bachmann [d], O. Karakas [d], M. Guillong [d], K. Molnár [e,f], I. Seghedi [g], Sz. Harangi [a,e]

[a] MTA-ELTE Volcanology Research Group, Pázmány P. sétány 1/C, 1117 Budapest, Hungary
[b] Department of Earth Sciences, University of Geneva, Rue des Maraîchers 13, 1205 Geneva, Switzerland
[c] Institute of Earth Sciences, Heidelberg University, Im Neuenheimer Feld 236, 69120 Heidelberg, Germany
[d] Department of Earth Sciences, ETH Zürich, Clausiusstrasse 25, 8092 Zürich, Switzerland
[e] Department of Petrology and Geochemistry, Eötvös Loránd University, Pázmány P. sétány 1/C, 1117 Budapest, Hungary
[f] Isotope Climatology and Environmental Research Centre, Institute for Nuclear Research, Hungarian Academy of Sciences, Bem tér 18/c, 4026 Debrecen, Hungary
[g] Institute of Geodynamics, Romanian Academy, 19–21 Jean-Louis Calderon St., R-020032 Bucharest-37, Romania

ARTICLE INFO

Article history:
Received 23 April 2020
Received in revised form 12 April 2021
Accepted 16 April 2021
Available online xxxx
Editor: R. Hickey-Vargas

Keywords:
zircon dating
magma storage
thermal model
magma flux
crystal mush
residence time

ABSTRACT

Ciomadul is the youngest volcano in eastern-central Europe. Although its last eruption occurred at ca. 30 ka, there are independent indications for a high-crystallinity magma reservoir persisting beneath the volcano until present. In order to further test the hypothesis of long-lived melt presence and to better constrain the nature and timescales associated with the subvolcanic magma storage system, over 500 zircon U-Th and U-Pb spot ages (crystal interiors and outer surfaces) were interpreted from dacitic rocks of the most productive eruptive period (the Young Ciomadul Eruptive Period; YCEP, 160-30 ka). Zircon surface ages from lava dome and pumice samples range from ca. 600 ka up to the youngest eruption event at 30 ka. They form a continuous age distribution and some single crystals reveal significant age zonation (>150 kyr difference from core to rim). The oldest zircon ages of YCEP overlap with the last eruption events of the Old Ciomadul Eruptive Period (1000–330 ka). The zircon age spectra, combined with textural data, point to a prolonged (several 100's kyr) residence in a highly crystalline mush state. The range in zircon crystallization temperature (from ~750 °C to the solidus at ~680 °C) is consistent with the results of thermometry on amphibole and plagioclase from felsic crystal clots, which represent crystal mush fragments. To maintain magma reservoir for such a long time above solidus, continuous magma input by deeper recharge is required. Zircon crystallization model calculations constrained by thermal modelling imply an average rate of magma input of about 1.3×10^{-4} km^3/yr over 2 Myr. Such estimate allows us to calculate an extrusive/intrusive ratio of 1:25–1:30. The model calculations suggest that a crystal mush zone of about 35 km^3 is still present within the subvolcanic magma reservoir. Importantly, the Ciomadul plumbing system thus remains thermally primed and renewed magma injection could lead to rapid reawakening and eruption of the apparently inactive volcano.

1. Introduction

Zircon provides valuable temporal, thermal and chemical information about the state of subvolcanic magma storage (see recent review by Cooper, 2019). Zircon geochronology contributed significantly to the understanding of vertically extensive, trans-crustal magmatic systems beneath volcanoes that could exist for duration of several 100's kyr (Reid et al., 1997; Wotzlaw et al., 2013, Caricchi et al., 2014, 2016; Cooper and Kent, 2014; Tierney et al., 2016; Cisneros de León and Schmitt, 2019). In combination with thermal modelling, zircon geochronology can provide essential quantitative

* Corresponding author.
E-mail addresses: reka.zsuzsanna.lukacs@ttk.elte.hu (R. Lukács), luca.caricchi@unige.ch (L. Caricchi), axel.schmitt@geow.uni-heidelberg.de (A.K. Schmitt), olivier.bachmann@erdw.ethz.ch (O. Bachmann), osgekarakas@gmail.com (O. Karakas), marcel.guillong@erdw.ethz.ch (M. Guillong), molnar.kata@atomki.mta.hu (K. Molnár), seghedi@geodin.ro (I. Seghedi), szabolcs.harangi@geology.elte.hu (Sz. Harangi).

https://doi.org/10.1016/j.epsl.2021.116965

information on the thermal evolution, accumulation and volume of eruptible magma in volcanic plumbing systems. A fundamental question that remains open is whether magmatic systems can contain some melt fractions for prolonged (several 10's to 100's kyr) time periods (e.g., Reid and Vazquez, 2017; Szymanowski et al., 2017) or whether they are mostly stored in a subsolidus state (e.g., Cooper and Kent, 2014; Rubin et al., 2017). Geophysical data are consistent with models suggesting that subvolcanic magma reservoirs are dominantly crystal-rich and contain a melt fraction, on average, between ~5 and 30% (e.g., Pritchard and Gregg, 2016). Zircon studies show that such conditions can last for prolonged period not only in large-volume, silicic magmatic systems (e.g., Toba, Okataina, Mogollon-Datil volcanic field; Cerro Galán; Bachmann et al., 2007; Folkes et al., 2011; Storm et al., 2011; Wotzlaw et al., 2013; Reid and Vazquez, 2017; Szymanowski et al., 2017), but it seems to also apply to andesitic and dacitic arc volcanoes (e.g., Mt St Helens, Lassen Peak; Claiborne et al., 2010; Klemetti and Clynne, 2014). The presence of potentially eruptible melt in the magmatic reservoir could lead to rapid reawakening (days to years; e.g. Burgisser and Bergantz, 2011; Druitt et al., 2012; Conway et al., 2020) and this poses an underrated risk particularly in case of long-dormant, apparently inactive, volcanoes. Thus, a better understanding of the temporal evolution of the thermal conditions within their magmatic systems is essential to estimate the potential whether they can erupt again.

Ciomadul is the youngest volcano in eastern-central Europe, with its last eruption occurring at ca. 30 ka (Harangi et al., 2010, 2015a, 2020; Szakács et al., 2015; Molnár et al., 2019). Yet, results of geophysical surveys, conductivity experiments and carbon-dioxide gas-monitoring campaigns are in agreement with the presence of a melt-bearing magma reservoir at subvolcanic depths (Popa et al., 2012; Harangi et al., 2015b; Kis et al., 2019; Laumonier et al., 2019). To further constrain the timescale of the magma storage system and the potential melt volumes in it, here we combine new zircon U-Th and U-Pb data with those published for the youngest volcanic units (Harangi et al., 2015a) and the oldest domes (Lukács et al., 2018). This data set now covers the entire 1 Myr long eruption history of Ciomadul in a statistically robust manner. Zircon age spectra serve as an important parameter in thermal modelling to constrain magma fluxes and volumes of magma reservoir at a given time (Caricchi et al., 2014, 2016; Tierney et al., 2016; Weber et al., 2020a). In this work, we have further refined zircon crystallization modelling and added Ti-in-zircon temperatures to better constrain the nature of the magmatic storage system and apply this technique for Ciomadul, a small-volume, long-dormant volcano. Our results show that a silicic magma reservoir with >100 km^3 in volume, mostly in a highly crystalline state, but with a significant proportion of melt can develop even at such volcanoes fed at relatively low magma flux ($<10^{-3}$ km^3/yr) over long periods of time (>1 Myr). Existence of sizeable eruptible magma pockets (with <~50 vol% crystals) beneath long-dormant volcanoes poses a greater potential hazard than previously appreciated.

2. Geological background

The Ciomadul volcanic dome field (CVDF) is the youngest manifestation of the volcanism in eastern-central Europe (Fig. 1). It is located at the southeastern end of the 160 km long Călimani-Gurghiu-Harghita volcanic chain. A comprehensive eruption chronology was reconstructed by combined (U-Th)/He, U-Th and U-Pb zircon dating (Harangi et al., 2015a; Molnár et al., 2018, 2019) and was supported by new K/Ar ages (Lahitte et al., 2019). Activity started with intermittent small volume lava dome extrusions with a cumulative erupted magma volume of ~1 km^3 in an area of 400 km^2 from 1 Ma to ca. 350 ka with long (>100 kyr) quiescence periods between eruptions (Old Ciomadul Eruptive Period; OCEP). Then, the eruptions focused on a more restricted area during the Young Ciomadul Eruptive Period (YCEP) from 160 to 30 ka, which is subdivided into two main eruptive epochs and several minor eruptive episodes that occurred at 160–150 ka (episode 4/1), 140–125 ka (episode 4/2), 105–95 ka (episode 4/3), 56–45 ka (episode 5/1), 35-30 ka (episode 5/2) and separated by quiescence periods lasting for ca. 15–40 kyr. The YCEP constructed the Ciomadul volcanic complex (CVC) with ~7 km^3 cumulative erupted magma volume. Extrusion of viscous magma occurred in distinct vents a few km apart and this lava dome complex was truncated by two deep explosion craters during the latest stage of the volcanism (Szakács et al., 2015; Karátson et al., 2016). The maximum eruption rate (~0.1 km^3/yr lasting over ca. 60 kyr) was reached during the Eruptive Epoch 4 of the YCEP (Molnár et al., 2019).

Compositionally, Ciomadul volcanism is characterized by a relatively homogeneous, crystal-rich (30–40 vol% crystals in the lava dome rocks and 20–25 vol% in pumices) high-K dacitic magma with dominantly plagioclase, amphibole and biotite phenocrysts (Seghedi et al., 1987; Vinkler et al., 2007; Kiss et al., 2014; Molnár et al., 2018, 2019). This differs significantly from the volcanic products of the pre-Ciomadul volcanism in South Harghita. The Ciomadul rocks have typically high abundance of Ba and Sr, depletion in Y and heavy rare earth elements and no negative Eu-anomaly. Amphiboles display significant compositional variations and zoning patterns suggesting interactions of compositionally variable magmas (Kiss et al., 2014; Laumonier et al., 2019; Harangi et al., 2020). Hornblende along with plagioclase macrocrysts crystallized at relatively low temperature of ~700–750 °C in an upper crustal felsic magma reservoir, whereas pargasitic amphibole formed at >900 °C from more mafic magmas (Kiss et al., 2014; Laumonier et al., 2019). Presence of high-Mg mineral phases, such as olivine, orthopyroxene and clinopyroxene in the dacites indicates that mafic magma recharge likely reactivated the felsic crystal mush (Vinkler et al., 2007; Kiss et al., 2014).

3. Methods

Samples already used for zircon dating (Harangi et al., 2015a; Lukács et al., 2018) were completed with additional ones from lava dome rocks and pumices. Now, this sample set represents the entire eruptive episodes of the YCEP. Zircon crystals were separated from crushed and sieved (<250 μm) bulk samples using standard density and magnetic separation techniques, followed by handpicking under a binocular microscope. Unpolished zircon surfaces (outer ~ 4 μm rims; depth profiling measurements) and sectioned interiors (mantles and rare visually identified cores based on CL images) were analysed for ^{238}U-^{230}Th geochronology by sensitive high resolution secondary ion mass spectrometry using a CAMECA ims 1280-HR ion microprobe at the HIP Lab of the Institute of Geosciences, Heidelberg University, Germany and a CAMECA ims1270 at the University of Los Angeles. Analysis protocols are detailed in Appendix Table A.1. Accuracy was monitored by interspersed analysis of AS3 and 91500 zircon reference materials in both laboratories. UCLA analyses on standards yielded a unity secular equilibrium ratio for $(^{230}Th)/(^{238}U) = 1.022 \pm 0.016$ (1σ, MSWD = 0.5; n = 8), whereas in case of the surface-analyses it was $(^{230}Th)/(^{238}U) = 0.981 \pm 0.015$ (1σ, MSWD = 2.2; n = 29). For the Heidelberg analysis session, secular equilibrium reference zircon analyses averaged $(^{230}Th)/(^{238}U) = 0.990 \pm 0.006$ (1σ, MSWD = 0.69, n = 33). Uranium concentrations were estimated from $UO^+/Zr_2O_4^+$ intensity ratios relative to zircon reference 91500 (U = 81.2 ppm; Appendix Table A.1). Model ages were calculated using the mean whole rock Th/U value of the Ciomadul dacites

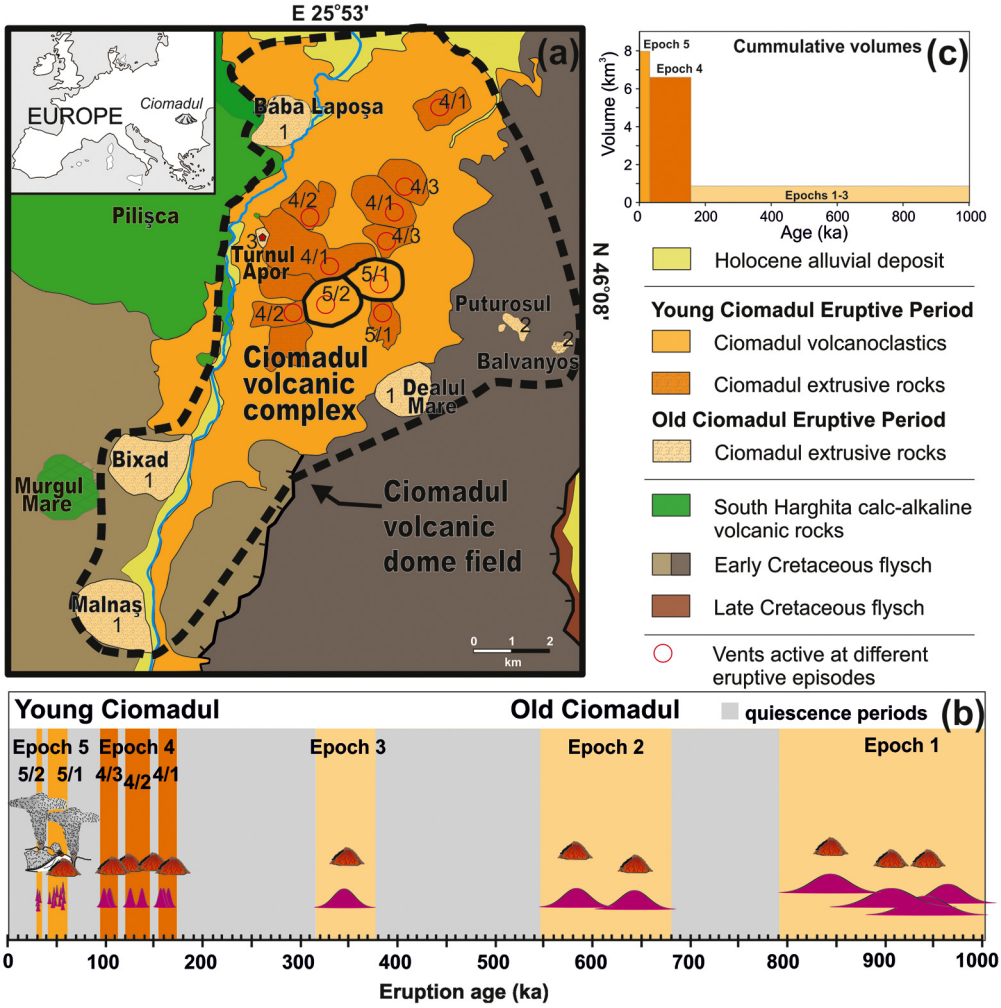

Fig. 1. a) Simplified map (original source: Seghedi et al., 1987) of the Ciomadul volcanic dome field (CVDF) and its surroundings. The twin craters of episodes 5/1 and 5/2 are outlined by bold black lines. b) Eruption chronology of the CVDF after Molnár et al. (2018, 2019), showing the epochs (and episodes) of the Young (YCEP) and Old Ciomadul Eruptive Periods (OCEP). Eruption styles, i.e. lava dome extrusion vs. explosive eruption are indicated above the eruption age curves (Gaussian probability, eruption age with uncertainties). c) Cumulative erupted volumes of the eruptive epochs (Szakács et al., 2015; Karátson et al., 2019; Molnár et al., 2019). (For interpretation of the colours in the figure(s), the reader is referred to the web version of this article.)

(3.58; Harangi et al., 2015a) and assuming secular equilibrium of the melt. Because the zircon-whole rock isochron slope is dominated by the zircon composition, variations in the melt composition within reasonable limits will not significantly change these model ages. In case of some secular equilibrium zircon domains, we additionally performed U-Pb analyses with the same SIMS instruments. Zircon U-Pb dates were corrected for initial disequilibrium of ^{230}Th using a constant D value of 0.33±0.06 (Rubatto and Hermann, 2007; Appendix Table A.1) to obtain internally consistent results with those published by Lukács et al. (2018).

Zircon trace elements including Ti, Y, Hf and REE analyses were performed by laser ablation inductively coupled plasma mass spectrometry (ICP-MS) at the Department of Earth Sciences, ETH Zürich with a Thermo Element XR SF-ICP-MS using 30 µm spot diameter (~10 µm depth) on the same samples analysed for in-situ geochronology. For additional information about trace element measurements see Appendix Table A.2. Because of the difference in sampling volume and the age heterogeneity within individual crystals, we did not correlate analyses for geochronology and geochemistry. The newly obtained YCEP trace element data were combined with the YCEP zircon age data from Harangi et al. (2015a) and OCEP zircon age data from Lukács et al. (2018). Additionally, we performed zircon trace element analyses also on these latter samples, using the same method as for YCEP zircons.

4. Results

Over 500 zircon U-Th (138 surfaces and 312 interiors) and U-Pb (65 interiors) spot ages from the youngest volcanic episode (YCEP) of Ciomadul were compiled in this study. These include 334 newly obtained geochronological analyses and already published data from some of the youngest eruption products (see Harangi et al., 2015a) and from one of the oldest lava dome of YCEP (KHM, Lukács et al., 2018). The new zircon analyses partly targeted the so far unrepresented lava domes of YCEP (epoch 4) and also extended the dataset to epoch 5 in order to get a statistically robust dataset, which covers most of the erupted materials of all the five YCEP eruptive episodes (Fig. 2, Appendix Table A.1).

In general, new results confirm the protracted crystallization timescale suggested by a more limited number of zircon dates from the youngest eruption products (Harangi et al., 2015a). In addition, this combined database provides evidence that zircon crystallization dates go back to ca. 600 ka. Age populations of individual eruptive episodes usually display a polymodal distribution with no apparent crystallization gap (within the uncertainty of the age data) in the probability density distribution curves constructed for each eruptive episode (Fig. 2). Importantly, the modes for crystal surface ages are very similar to those derived from interiors, albeit interior ages are slightly offset to older ages. However,

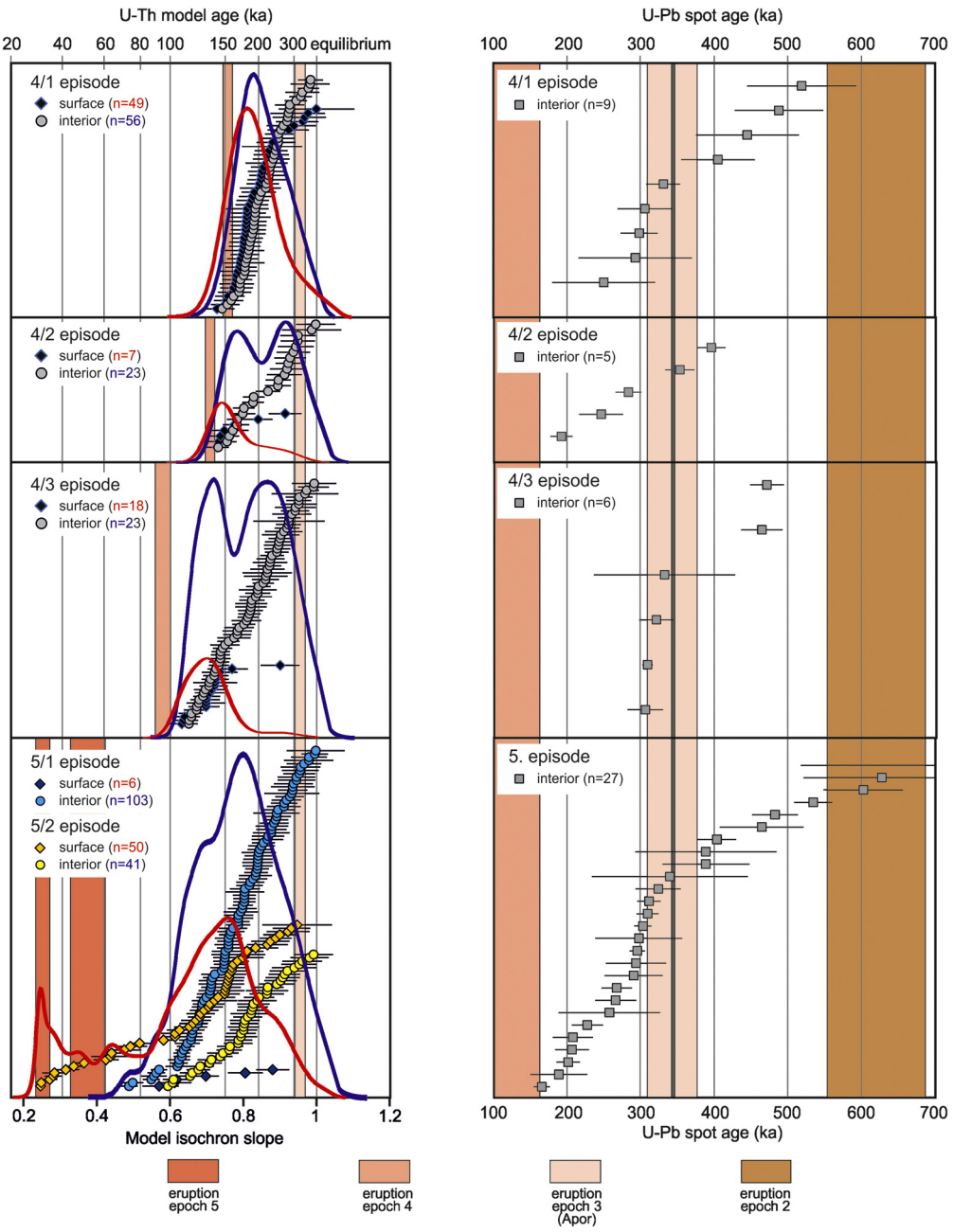

Fig. 2. Rank order plots for U-Th model ages (represented as model isochron slopes to incorporate 1σ uncertainty symmetrically; left panel) and for U-Pb spot ages (right panel; 1σ uncertainty) of zircon interiors and surfaces from the YCEP samples. The U-Th model ages are superimposed by probability density population curves (red: zircon surfaces; blue: zircon interiors) obtained by DensityPlotter (Vermeesch, 2012). Eruption ages of eruption epochs (Harangi et al., 2015a; Molnár et al., 2018, 2019) are shown by coloured vertical bars.

where multiple analysis spots were placed onto crystal interiors, they often display significant younging from core to rim (Appendix Fig. A.1). Within individual grains, spot ages range over several 10's to even 100's kyr (Appendix Fig. A.1). Although our dataset is certainly biased towards dates $<$350 ka (as we performed mostly U-Th analyses and limited U-Pb dating), we found only few dates $>$400 ka (Fig. 2). The majority of the obtained U-Th model dates are between 350 ka and 100 ka and only $<$10 % fall between 100 and 30 ka.

Statistical deconvolution of zircon surface crystallization age spectra using the mixing model of Sambridge and Compston (1994) identifies modes (Appendix Fig. A.2) for the eruptive episodes between 160 and 95 ka (epoch 4), predating the eruption age by about 10-40 kyr. This is also the case for the youngest eruptive epoch 5 (57–30 ka), but zircon rim and interior crystallization ages display more complex distributions compared to those of epoch 4 due to the intrinsically smaller U-Th age uncertainties for younger crystals. The dominant age populations in epoch 5 lie between 200 and 100 ka ($\sim$75%), whereas only a limited subset ($\sim$12%) of surface ages is $<$75 ka. Four modes at 33$\pm$1 ka, 62$\pm$2 ka, 114$\pm$1 ka and 176$\pm$1 ka are identified. Although the identification of age modes depends on the number of zircon dates and their precision which often limits their significance (Kent and Cooper, 2017). We used Kolmogorov–Smirnov statistical testing to compare zircon age populations of successive eruptive episodes (Appendix Fig. A.3). We found that in all cases the compared populations were indistinguishable at the 95% confidence level. Noteworthy, the progressively younger volcanic formations contain

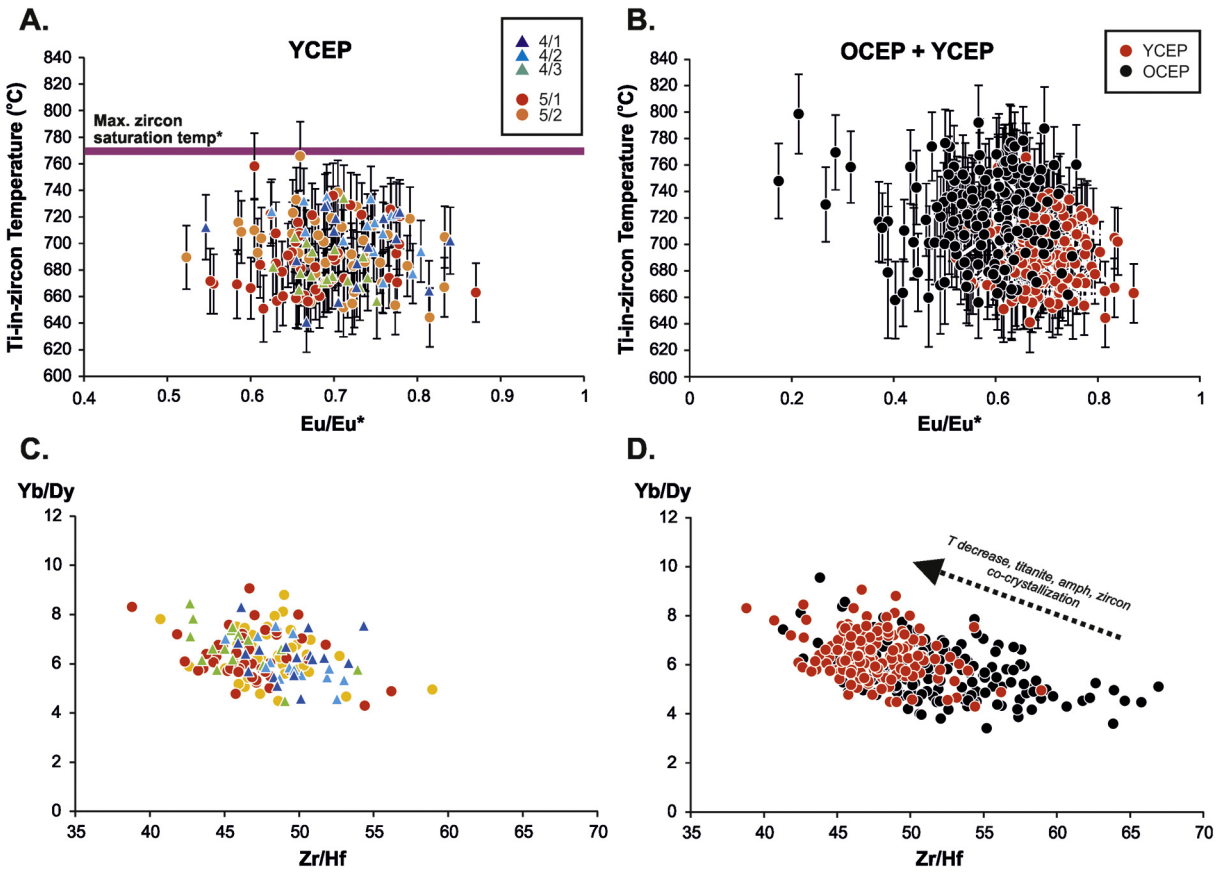

Fig. 3. Zircon geochemical signature of distinct eruptive episodes (from 4/1 to 5/2) of YCEP in the left panels (A, C) and comparison of the YCEP and OCEP zircon chemistry at right panels (B, D). Ti-in-zircon temperatures (Ferry and Watson, 2007) were calculated using $a_{TiO2} = 0.6$ and $a_{SiO2} = 1$. Zircon saturation temperature was calculated from glass chemistry of the youngest eruption products of the YCEP (Harangi et al., 2020) following the method of Boehnke et al. (2013). Using the two end-member glass composition data of Harangi et al. (2020), the calculated zircon saturation temperature values are in the range between 710 and 770 °C. In Fig. 3A, the maximum zircon saturation temperature is shown.

zircons with the age population found in the previous eruption products. This suggests a common long-lived magma reservoir, in which successive volcanic episodes were fed by magmas containing newly crystallized and older zircon population. Overall, this continuous recycling produces a wider range of zircon crystallization ages in younger eruptions compared to the older episodes.

The chemical composition of the YCEP zircons shows similar variability throughout the episodes of volcanic activity between 160 and 30 ka (Appendix Table A.2; Fig. 3; and Appendix Figs. A.4-6). The Hf concentrations in the analysed crystals range from ~8500 to 11500 ppm, and Eu/Eu* is between 0.5 and 0.9 (mostly between 0.6 and 0.8; Fig. 3A), indicative of co-crystallizing zircon, plagioclase and titanite. The Yb/Dy values cluster between 4.5 and 9, correlating positively with Hf concentrations, and negatively with Th/U (Fig. 3). Th/U ratio of zircon depends primarily on the melt composition and therefore, reflects how evolved the melt fraction is from which zircons crystallized (Reid et al., 2011; Reid and Vazquez, 2017). Ciomadul YCEP zircon displays Th/U between 0.4 and 1.5, with about 80% of data falling in the range from 0.4 to 0.8 (Appendix Fig. A.5). Such values indicate crystallization primarily from evolved, rhyolitic melt, and zircon with higher values (>0.8) formed from a less silicic, dacitic melt.

The Ti-in-zircon thermometer (Ferry and Watson, 2007) was applied using $a_{TiO2} = 0.6$ and $a_{SiO2} = 1$ to infer zircon crystallization temperatures. The TiO_2 activity value is estimated based on the glass Ti contents using the methodology of Hayden and Watson (2007; Appendix A). In all eruptive episodes, a fairly uniform temperature range between 650 and 740 °C (mean = 693±25 °C; Appendix Fig. A.4) is obtained. The temperature values show a positive correlation with Th/U, and negative correlations with Hf and Yb/Dy, but no systematic variation with Eu/Eu* (Fig. 3). Zircons from the older, 1000–330 ka eruptive period (OCEP; Appendix Table A.2; Fig. 3; Appendix Figs. A.4-6) have similar trace element composition to YCEP zircons, but with more variance and slight overall shifts to higher crystallization temperatures (~650–780 °C; mean = 720 ±32 °C; Appendix Fig. A.4), lower Hf (7000–11000 ppm), Yb/Dy (3.4–9.6; Fig. 3), Eu/Eu* (0.17–0.83; Fig. 3), Ce/Ce* (Appendix Fig. A.6) and higher Th/U (0.23–1.79; Appendix Fig. A.5).

5. Modelling zircon crystallization

Rate of magma input and the thermal state of the crust are primary factors controlling the nature of subvolcanic plumbing systems, including the volume of eruptible magma (Annen et al., 2006; Annen, 2009; Karakas et al., 2017; Weber et al., 2020b). The duration of zircon crystallization, i.e. the zircon age spread has shown to be a key proxy to constrain the magma fluxes by the comparison with modelled zircon age distributions obtained from thermal modelling (Caricchi et al., 2014; Weber et al., 2020a). The statistically robust zircon data set of Ciomadul provides an excellent opportunity to investigate the thermal history of a magma reservoir beneath a small-volume volcanic system. Thermal model calculations simulating the prolonged injection of magma in the crust were performed using the method described in Karakas et al. (2017) and Laumonier et al. (2019). Magma is injected incrementally in the crust over the estimated lifetime of the magmatic system (i.e. 2 Myr). Heat conduction between the crust and intruded magmas over time is investigated by a two-dimensional, fully im-

plicit, forward, transient heat diffusion code using a finite volume scheme (Patankar, 1980). We consider a two-dimensional domain (60 km × 60 km) with a 40 km thick crust having a steady-state geotherm with 0 °C surface temperature and constant heat flux at the mantle-crust boundary. We emplaced dikes and sills incrementally and randomly using a stochastic and instantaneous scheme over a total of 4 Myr into the lithosphere following a two-stage process. First, basaltic magmas were emplaced in the lower crust for 2 Myr, which increases the temperatures of the entire crust (geothermal gradient was elevated by about 20% with respect to the normal one). In the second stage, the model switches to intrusion of dacitic magmas into the upper crust (7–15 km depths; injection temperature 950 °C). The silicic magma is considered to represent the product of fractionation of basaltic magma in the lower crust. The calculated duration of zircon crystallization is essentially controlled by the rate of heat (i.e. magma) input into the crust. Thus, a decrease of the temperature of the injected magma can shorten the period over which zircon crystallizes. However, the decrease of enthalpy content of magma for a decrease of temperature with 50 °C is only of the order of 3% (Caricchi and Blundy, 2015). This implies that our flux estimates would vary by only a few percent considering temperatures for the injected magma that are within about 100 degrees from the temperature used for this study. Passive tracers (40 m × 40 m), added with the magma, record the evolution of temperature in time in different portion of the system. The number of tracers with each intrusion varies but their total number is always larger than 300. The rate of magma input in the crust was between 10^{-2} and 10^{-4} km^3/y.

We use the time-temperature record of each tracer to calculate the number of zircon crystallization ages available for analysis (Fig. 4). The number of measurable zircon ages varies proportionally to the rate of zircon crystallization following the parameterization proposed by Tierney et al. (2016). As a consequence, a smaller number of measurable ages is calculated when the temperature of a tracer approaches the solidus (Appendix Fig. A7). Zircons are modelled to grow from a maximum temperature that can vary between 770 °C down to solidus temperature (∼650 °C). We assume that at the moment of eruption, all tracers with a temperature within the zircon crystallization range are erupted. This implies that all tracers that cooled below solidus before eruption will not contribute to the final distribution of measurable ages sampled by an eruption (Fig. 4). The model neglects convection within the reservoir, as the effect of convection on the thermal evolution of the magmatic system has been shown to be minor (Caricchi et al., 2014, 2016). High frequency modulation of magma fluxes (which are in fact simulated in our model where the input rate changes from infinity during injection to 0 during breaks), are not visible in the modelled population of zircon ages for two main reasons: the thermal inertia of a magmatic system and the analytical uncertainty that smoothes the distribution of zircon ages. Other sensitivity tests were already performed in Caricchi et al. (2014, 2016).

Our calculations show that with increasing rate of magma input, tracers spend longer time within the zircon crystallization range and therefore the range of ages over which continuous zircon crystallization is recorded increases with magma flux (Fig. 4). Additionally, at the highest fluxes, few tracers that initially cooled below solidus are re-heated before eruption to temperatures compatible with zircon crystallization. The average temperature of the tracers (i.e. of the magma eventually sampled by an eruption) initially increases and then reaches rather constant values in all models (Fig. 4). The rate of temperature increase at the beginning of the model depends on the magma flux. The plateau value of average temperature along with its standard deviations in the different models decreases slowly with time: the rate of this decrease again depends on the average rate of magma input (Weber et al., 2020a).

6. Discussion

6.1. Episodic vs. continuous zircon crystallization

Zircon age distributions are often difficult to interpret in terms whether they indicate episodic or continuous crystallization (Kent and Cooper, 2017). Due to the uncertainties of the U-Th model dates, brief (less than few thousand years) perturbations in magma temperature or chemistry cannot be resolved. A hiatus in zircon crystallization could be due to various processes (Reid and Vazquez, 2017):

1. local Zr depletion in the surrounding melt, especially under conditions where melt convection ceased (little to no replenishment of fresh magma);
2. increasing temperature above Zr-saturation or mixing with Zr-undersaturated melt during recharge (inducing resorption);
3. zircon entrapment by a major phenocryst phase, or into a subsolidus part of the magma reservoir.

Episodic vs. continuous zircon crystallization is usually interpreted based on various statistical techniques such as probability and kernel density distributions of zircon ages, isochron slopes or the Sambridge and Compston (1994) mixture modelling. Frey et al. (2018) suggested episodic zircon crystallization separated by long subsolidus conditions for the youngest volcanism of Dominica (Lesser Antilles) based on the hiatuses observed in the zircon spectra. In contrast to the punctuated zircon age distributions shown by Frey et al. (2018), the Ciomadul zircon surface dates lack pronounced gaps in the age distributions. However, we cannot exclude the possibility that punctuated crystallization was occurring on timescale shorter than the uncertainty on zircon age determinations (i.e. in <10 kyr scale). Within the magmatic zoning, only inconspicuous resorption surfaces are occasionally present, suggesting partial dissolution and renewed crystallization of zircon crystals, possibly due to magma recharge. Local chemical depletion of the melt (Reid and Vazquez, 2017), interrupting zircon crystallization, could also occur due to high crystallinity (>40–50 vol%) in the magma reservoir, suppressing bulk magma convection. Lulls in zircon crystallization can be caused by pre-eruptive heating above the zircon saturation temperature (710–770 °C; Fig. 3.), and this might be indicated by zircon surface ages significantly (with a few 10' kyr) predating the eruption. This is recognized for several of the Ciomadul samples (Harangi et al., 2015a) and also for other volcanic systems (e.g., Friedrichs et al., 2020; Gençalioğlu-Kuşcu et al., 2020; Weber et al., 2020a). Pre-eruptive reheating may stop zircon crystallization or even dissolve the outermost zircon layers. Alternatively, very thin new overgrowths may go undetected when integrating data over the outer ∼4 μm deep crater generated during SIMS depth profiling. Furthermore, newly formed zircon crystals growing just before eruption might be too small for separation and therefore may be underrepresented in the obtained zircon ages.

Based on zircon age spectra and textural evidence, the favoured scenario for Ciomadul is prolonged (over several 100's kyr) zircon crystallization in a long-lived, mostly highly crystalline mushy environment with limited convection, where occasional interruptions in zircon crystallization were due to localized recharge, Zr depletion in the melt or shielding by solidification. The successive zircon U-Th and U-Pb dates from the YCEP dacites overlap within analytical uncertainties in ranked order distribution plots (Fig. 2). Thus, the zircon age spectra are permissive of protracted and quasi-continuous crystallization (>350 kyr). Both interior and surface zircon ages record long crystallization histories for each eruption and hence the overall timescale of zircon crystallization

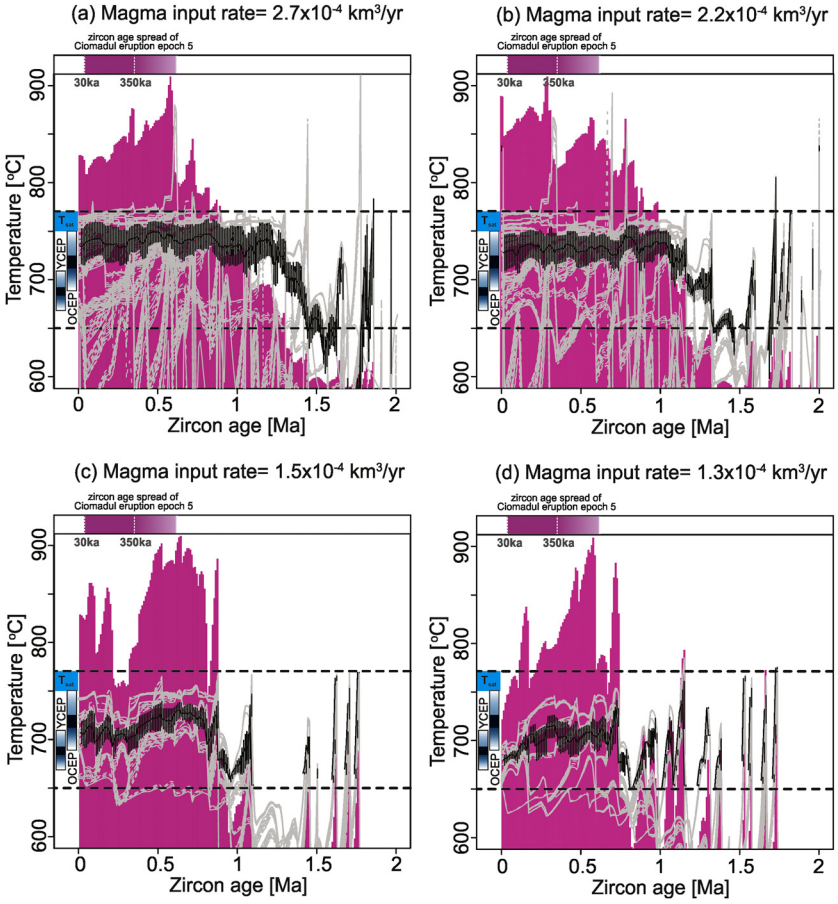

Fig. 4. Results of the thermal modelling performed for different magma input rates (decreasing from panel a to d). The grey lines show the evolution of the tracers that are within the zircon saturation temperature range after 2 Myr of magma injection (time increasing from right to left). The black lines and the bar show the evolution of mean temperature and standard deviation during the 2 Myr of magma injection, respectively. The histogram in pink shows the calculated distribution of potentially detectable zircon ages since the onset of magma injection (note y axis shows the relative frequency in this case). The dashed line represents the range of zircon saturation temperature used for the calculations. The bars above the panels show the zircon age spread in the samples of eruption epoch 5 within the YCEP. Note that ages >350 ka are underrepresented, as U-Pb dates are limited in the data set. The age spread of the natural zircon data has the best fit with the modelled duration for the lowest magma input rate (panel d). Average zircon crystallization temperatures with the standard deviation calculated based on Ti-in-zircon thermometry data (Appendix Fig.A.4) for the YCEP and OCEP, respectively, as well as the calculated zircon saturation temperature range (Fig. 3) are presented on the left side of the diagrams for comparison to the modelled average temperature.

can be considered as a robust indication of magmatic longevity within the temperature range where zircon is saturated. Quasi-continuous zircon crystallization is also evident from individual crystals, including those from a ca. 95 ka old lava dome. A progressive rimwards younging is observed for multiple analysis spots on different crystals, which yielded ages that decrease from 293 ka to 128 ka (Appendix Fig. A.1). This suggests that zircon crystals were in contact with melt at least intermittently throughout their residence time and thus, a significant part of the magma storage occurred at temperatures above the solidus. In this sense, crystallization can be regarded as continuous (i.e. without hiatuses significantly longer than the uncertainty on single age determinations) in the reservoir as a whole. In order to generate statistically significant hiatuses in the distribution of zircon ages, gaps in zircon crystallization (or zircon resorption) would have to be extensive to affect a large portion of the magma reservoir, which, however, is not observed in the distribution of zircon ages.

To maintain a long-lived reservoir above its solidus, continuous magma input, i.e. repeated magma recharge is required. Although the Ciomadul magma storage system was maintained via recharge events for protracted time, episodically more intensive magma input (e.g., >200 °C reheating before the 135 ka Ciomadul Mic lava dome extrusion; Kiss et al., 2014) likely triggered eruptive events.

6.2. Zircon crystallization in a long-lasting subvolcanic magma reservoir

The common occurrence of low temperature (650–750 °C) mineral assemblages and felsic crystal clots with inter-crystalline glasses in the Ciomadul dacites suggest that at least part of the subvolcanic magma reservoir was kept at high crystallinity (Kiss et al., 2014). Periodic recharge events led to partial remelting of the major mineral phases (mostly plagioclase, amphibole and biotite), rejuvenating parts of the reservoir to become eruptible. Eruption of magma occurred from well-mixed domains within the magmatic system with antecrystic major and accessory minerals. Zircon populations with various crystallization ages formed during episodic mush reorganization that not necessarily caused eruption but coalescence of distinct parts of the reservoirs during convecting stirring episodes (Vazquez and Reid, 2004; Bachmann and Bergantz, 2006).

The efficiency of pre-eruptive rejuvenation is reflected by the wide range of zircon dates in all samples. The heterogeneity of zircon ages and variation in trace element compositions in single hand-samples imply that multiple zircon generations became successively mixed and ultimately entrained into the erupted magma. Bulk rock compositions are fairly homogeneous and variations in zircon chemistry are similar in each eruption product (Fig. 3

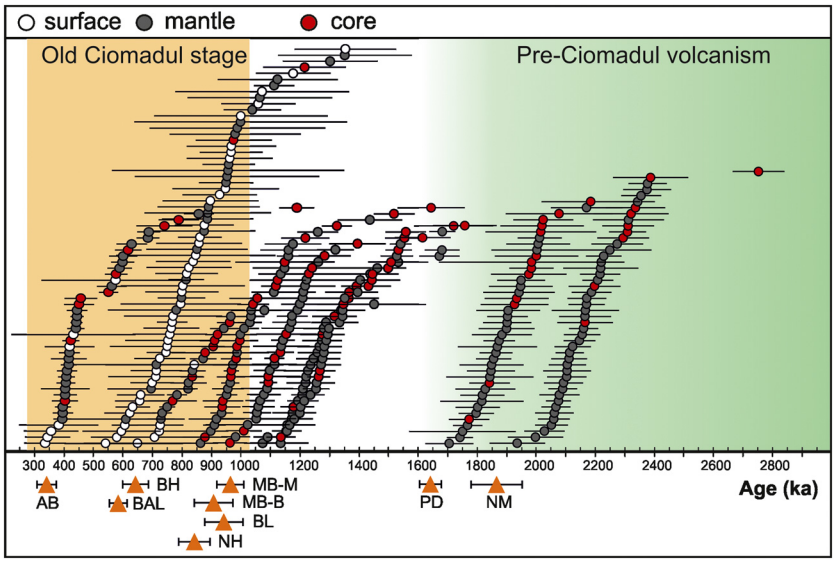

Fig. 5. Zircon crystallization ages (with 2se uncertainty) of OCEP eruption products based on U-Pb geochronology data of Lukács et al. (2018). The orange triangles below the main diagram represent the eruption ages (cf. Fig. 1) with uncertainties given by Molnár et al. (2018). Abbreviations: AB = Turnul Apor; BAL = Balvanyos; BH = Puturosul; NH = Dealul Mare; BL = Baba-Laposa; MB = Bixad; MB-M = Malnaș; PD = Pilișca; NM = Murgul Mare (Fig. 1).

and Fig. A.5 in Supplementary Material), suggesting efficient pre-eruption mixing in the magma reservoir. Glass major element data (matrix glass and silicate melt inclusions; Vinkler et al., 2007; Harangi et al., 2020; Karátson et al., 2016; Laumonier et al., 2019) of the eruptive products are rhyodacitic to rhyolitic and such compositional variation is supported also by the mineral cargo showing considerable compositional range (e.g., amphiboles; Kiss et al., 2014; Laumonier et al., 2019). Zircon Th/U values in each eruption product vary widely implying mixed crystal populations that are derived from variously evolved silicic melt fractions in the crystal mush body. Zircon crystals are expected to occur mostly immersed in the melt phase because of their small size (Reid et al., 1997; Bindeman, 2003; Claiborne et al., 2010), and they remain stable for protracted durations at the dominantly low, near solidus temperature (700-750 °C) of the crystal mush. This is supported also by the results of thermal modelling which indicate rather constant average temperatures (650–750 °C; Fig. 4) in the crustal magma reservoir for 100's of thousands of years.

Rejuvenation events were likely brief, particularly when high temperature mafic magmas were injected into the crystal mush reservoir. The bimodality of the amphibole population (Kiss et al., 2014; Laumonier et al., 2019) in the dacites suggests that the erupted magmas contained a mixture of components from the low-temperature felsic mush and the hot recharge magmas. Noteworthy, we have not found zircons with relatively high temperature (>750 °C) nor strong resorption within zircon crystals, suggesting rapid pre-eruption reactivation. Nevertheless, if the system is highly crystallized, magma injection does not necessarily result in an increase of temperature because all heat is consumed for melting the crystals.

Similarly long-lived magma reservoirs have been identified for other andesitic to dacitic volcanic systems such as Mount St Helens (Washington, USA; Claiborne et al., 2010), Lassen Peak (California, USA; Klemetti and Clynne, 2014), Nevado de Toluca, Mexico (Weber et al., 2020a), the Altiplano-Puna Volcanic Complex (Central Andes; Kern et al., 2016; Tierney et al., 2016), the Soufriére volcano (St. Lucia, Lesser Antilles; Schmitt et al., 2010) and the Mt. Erciyes (Central Anatolia, Turkey; Friedrichs et al., 2021), as well as for the large volume Fish Canyon Tuff (Colorado, USA; Bachmann et al., 2007; Wotzlaw et al., 2013) and Younger Toba Tuff, Indonesia (Vazquez and Reid, 2004; Reid and Vazquez, 2017). Although these volcanic systems yielded magma volumes in scale from 10 to the few 1000 km^3, they all have a common feature that these eruptions tapped cool (just above the solidus) and wet calc-alkaline silicic magmas (Lipman and Bachmann, 2015; Reid and Vazquez, 2017). This feature holds also for the Ciomadul dacites (Kiss et al., 2014; Laumonier et al., 2019).

6.3. Relations to the older magma reservoirs

Within the studied zircon population of the YCEP samples, there are some zircon interiors crystallized before the 344±33 ka Apor eruption (Molnár et al., 2018), the last known eruption in the OCEP phase (Fig. 2 and 5). Thus, they are presumably derived from its precursor magma body. Much older zircon crystals (derived from Epoch 1 and 2 of OCEP, Fig. 5), on the other hand, are scarcely observed in the YCEP samples. This can be explained either by the peripheral and isolated position of the OCEP magma reservoirs beneath the Ciomadul volcanic dome field except for Apor dome that is within the CVC (Fig. 1) or because these reservoirs were already solidified at the time of the YCEP eruptions. Thus, the YCEP subvolcanic magma body can reasonably be interpreted as the continuation of the Apor system that existed during the apparently long eruption hiatus before YCEP volcanism (ca. 160 ka; Molnár et al., 2019). The Apor eruption contains zircon with ages >500 ka, which cover the eruption and zircon crystallization ages of the previous OCEP Epoch 2 eruptions (Fig. 5). All preceding eruption materials of OCEP show overlapping zircon age spreads. This implies a continuity of magma storage and efficient recycling of OCEP intrusions in the subsequent eruptive epochs.

The apparent continuity between OCEP and YCEP systems has two important implications: 1) zircon crystallization already started ≥1.5 Ma ago; 2) the spatial overlap between eruption centres within the CVDF since the Apor eruption suggests homogenization of a common magma reservoir where zircon with different ages became efficiently mixed before eruptions. Therefore, we propose that the ~100 km^2 CVDF represents the subaerial manifestation of an extensive magma reservoir in the upper crust that has built up over 1.5–2 Myr. This occurred in an already slightly heated crust as a result of the nearby Pilișca volcanism (Fig. 1; Pre-Ciomadul volcanism). Although some parts of this magma reservoir became certainly solidified, there were always portions with sufficient melt present that allowed episodic rejuvenation and eruption.

The thermal condition of the long-lived magma reservoir beneath Ciomadul during the YCEP stage appears to have been fairly low, as indicated by the generally low Ti content of zircons (Appendix Figs. A.4 and A.6) and the abundance of a felsic mineral assemblage with compositions indicative of crystallization at relatively cold environment (<750 °C; Kiss et al., 2014). This is consistent with prolonged existence of a felsic crystal mush just above the solidus that was growing by progressive magma input (Caricchi et al., 2014). Felsic glomerocrystic crystal clots (consisting of plagioclase, low-Al amphibole, biotite, accessory minerals such as titanite, zircon and apatite as well as occasional quartz and K-feldspar; Kiss et al., 2014) occur frequently in the dome rocks and they are inferred to represent this evolved crystal mush material. The inter-crystalline vesiculated glass has mostly rhyolitic compositions (Laumonier et al., 2019) and represents the evolved melt fraction in the crystal mush, where zircons remained stable for a long time. On the other hand, zircon from the OCEP stage has slightly higher Ti abundances and trace element signatures indicating derivation from less evolved melt compared to YCEP zircon (Fig. 3; Appendix Figs. A.5-6). These rocks show a larger variability in bulk rock composition (Molnár et al., 2018) and typically have plagioclase and amphibole pairs (Harangi et al., unpubl. data) providing higher crystallization temperatures than those in the YCEP dacites. Thus, there is a temporal shift to more evolved and homogeneous magma and lower temperature condition from OCEP to YCEP. Based on the model results discussed below, this suggests that the system has grown with time, leading to an increasingly homogeneous magma composition characterized by relatively constant and low temperatures consistent with the results of Weber et al. (2020b).

6.4. Maintaining the protracted Ciomadul reservoir based on thermal modelling

The zircon U-Pb and U-Th model ages show that all YCEP eruptions between 160 and 30 ka sample zircon up to 600-500 ka old and that the zircon age range increases for progressively younger eruptions. This means that in addition to newly crystallized zircon, antecrysts from earlier episodes were recycled (Fig. 2). Such an age spread suggests quasi-continuous zircon crystallization over a protracted (several 100's kyr) timescale and effective pre-eruption mixing within the Ciomadul magma reservoir. Although Kent and Cooper (2017) proposed that uncertainties of individual zircon ages preclude assigning unique thermal histories to such data, Weber et al. (2020a) showed that the reliability of natural zircon age distributions strongly depends on the sampling size. Therefore, the total duration of quasi-continuous zircon crystallization (as recorded by the zircon age spread) and the average temperature within the magma reservoir (reflected by the crystallization temperatures calculated by Ti-in-zircon thermometry as well as major mineral thermometry; this study and Kiss et al., 2014; Laumonier et al., 2019) are solid proxies to estimate the thermal evolution and average rate of magma input into the plumbing system and the volume of melt within the reservoir (Fig. 4). We considered that the pre-Ciomadul volcanism already heated up the crust. Noteworthy, none of the Ciomadul eruption sampled zircons from the older (>1.65 Ma) magma reservoir and the Ciomadul magma has also a distinctive compositional feature compared to the >1.65 Ma andesitic to dacitic rocks of South Harghita (Molnár et al., 2018). Thus, the Ciomadul magma system developed independently from the older volcanism but in an area with an already elevated geothermal gradient. The relatively homogeneous composition of the erupted products since 600 Ma (epoch 2; Molnár et al., 2018, 2019) also suggests an elevated geothermal gradient already at the beginning of volcanism, otherwise with the low magma flux indicated by our model more time would be required both to match the spread of zircon ages and their measured chemical homogeneity (Weber et al., 2020b).

The total spread in zircon ages sampled by the last eruption stage (eruptive epoch 5) of Ciomadul is about 600 kyr and the model that produces a similar spread in zircon ages is that for the lowest average rate of magma input tested here (1.3×10^{-4} km^3/yr; Fig. 4d). Further support for this relatively low rate of magma input comes from crystallization temperature estimates. The calculations performed with this rate of magma input show that the average temperature over the last 0.5 Ma should be between 670 and 720 °C, which is remarkably similar to that obtained by the Ti-in-zircon as well as the major mineral thermometers (Figs. 3 and 4d). Higher magma fluxes would produce longer periods of continuous zircon crystallization and higher average temperature estimates. As an example, if the magma flux was two times higher (i.e. 2.7×10^{-4} km^3/yr), zircons ages could spread over about 1.5 Ma, with average temperatures of the order of 720-750 °C (Fig. 4a). As lower rates of magma input in the crust over longer timescales (i.e. >2 Ma) could potentially also yield a similar spread in zircon ages and average temperatures, 1.3×10^{-4} km^3/yr is considered as a maximum estimate. This estimated magma flux is significantly lower than calculated for Nevado de Toluca volcano (Mexico), which was active for a comparable timespan as Ciomadul, but produced six-times larger erupted magma volume (60 km^3; Weber et al., 2020a).

At the preferred model rate of 1.3×10^{-4} km^3/yr magma flux, about 260 km^3 magma was injected in the upper crust over 2 Myr. The melt fraction in this reservoir and the volume of the eruptible magma were calculated for this timespan based on the thermal model presented in this study. The volume of the eruptible magma (i.e., the magma fraction having >50% melt at >800 °C) along with the fraction of supersolidus, but uneruptible material (high crystallinity mush at >670 °C) in the reservoir both increase with time and just before the eruptive epoch 4 they reach ~6 km^3 and 35 km^3, respectively (Fig. 6). This is consistent with the productivity of epoch 4 resulting in 4–5 km^3 cumulative volume of extrusive material for a timespan of 70 kyr from 160 to 90 ka (Szakács et al., 2015; Karátson et al., 2019; Molnár et al., 2019). Intermittent evacuation of small volumes of magma are negligible for the thermal state of the entire magma reservoir and the eruptive loss of magma is compensated by injection of fresh magma. This means that sufficient potentially eruptible magma remained after 40 kyr of dormancy at the onset of the eruptive epoch 5. For continued magma injection, we suspect that similar conditions exist presently beneath Ciomadul as supported by seismic and magnetotelluric models (Popa et al., 2012; Harangi et al., 2015b). The estimated magma and melt volume derived from thermal modelling of zircon crystallization is comparable, although a little bit lower, than calculated by Laumonier et al. (2019) based on magnetotelluric results and conductivity experiments. The comparatively small volume of erupted material produced by Ciomadul so far (ca. 8–10 km^3 as determined by Szakács et al., 2015; Karátson et al., 2019; Molnár et al., 2019) results in an extrusive-intrusive ratio of 1:25 to 1:30, lower than the 1:1 to 1:16 ratio of average continental volcanism (White et al., 2006), but higher than the 1:75 ratio proposed for the waning stages of the Altiplano-Puna magma system (Tierney et al., 2016). Remarkably, based on seismic and stratigraphic data, similar volcanic to plutonic ratios were calculated for Pinatubo (Mori et al., 1996; Wolfe and Hoblitt, 1996) and Nevado del Toluca (Weber et al., 2020a), which produced dacitic volcanic rocks akin to Ciomadul.

The dacitic upper crustal reservoir of Ciomadul seems thermally primed and therefore potentially capable of mobilizing up to a few km^3's of eruptible magma upon recharge. Injection of hot mafic magma as evidenced by petrology and mineral chemistry of the past eruption stages (Kiss et al., 2014; Laumonier et

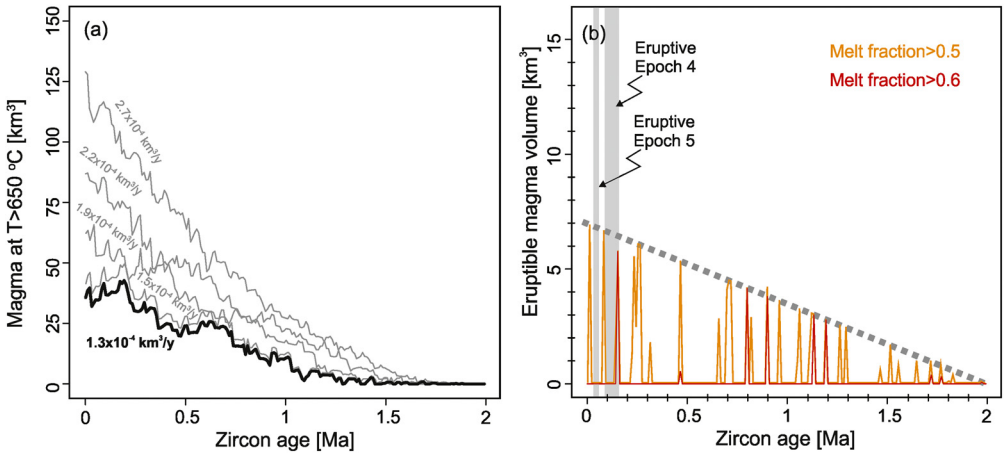

Fig. 6. Time evolution of supersolidus and eruptible magma volumes in the Ciomadul magmatic system based on thermal modelling results. a) Volume of magma above solidus calculated for the simulated range of magma fluxes. The inferred 1.3×10^{-4} km^3/y magma flux over 2 Myr led to around 30-40 km^3 magma in supersolidus state within the magma reservoir of estimated 260 km^3 volume. b) Volumes of eruptible magma containing in excess of 0.5 (orange) and 0.6 (red) melt fraction. The spikes correspond to the random injection of a new sill into the plumbing system. Note that the magma system is capable to produce continuously larger volume of eruptible magma reaching 6 to 7 km^3 when the eruptive epoch 4 and 5 occurred at Ciomadul.

al., 2019) is a powerful trigger mechanism causing rapid (within months to years) rejuvenation. Further research is necessary as apparently inactive volcanoes with primed magma reservoirs like Ciomadul could revive fast even after long (in human terms) periods of quiescence, which has significant implications for volcanic hazard assessments. Our results urge attention to other areas with long-dormant volcanoes, which could have unnoticed, but long-living and still active subvolcanic magma reservoir.

CRediT authorship contribution statement

R. Lukács: Conceptualization, Formal analysis, Investigation, Methodology, Visualization, Writing – original draft. **L. Caricchi:** Formal analysis, Investigation, Methodology, Software, Writing – review & editing. **A.K. Schmitt:** Data curation, Writing – review & editing. **O. Bachmann:** Writing – review & editing. **O. Karakas:** Investigation, Software. **M. Guillong:** Data curation. **K. Molnár:** Resources, Writing – review & editing. **I. Seghedi:** Writing – review & editing. **Sz. Harangi:** Supervision, Visualization, Writing – review & editing.

Declaration of competing interest

The authors declare that they have no known competing financial interests or personal relationships that could have appeared to influence the work reported in this paper.

Acknowledgements

The authors thank to the members of the MTA-ELTE Volcanological Research Group (Budapest) for their helps during the field and laboratory works. I. Seghedi benefited by a grant of the Ministry of Research and Innovation, CNCS–UEFISCDI, project no. PNIII-P4-ID-PCCF-2016-4-0014, within PNCDI III and R. Lukács benefited by the János Bolyai Research Scholarship of the Hungarian Academy of Sciences. The HIP facility at Heidelberg University is operated under the auspices of the DFG Scientific Instrumentation and Information Technology programme. We are very grateful the three reviewers, Mary Reid, Mark Stelten and Casey R. Tierney for the constructive comments and suggestions, which helped to clarify our results.

Funding: This work belongs to the research projects supported by the National Research, Development and Innovation Office in Hungary (No. K116528, No. PD 121048 and No. K135179); the European Union, KMP project (No. 4.2.1/B-10-2011-0002); and the European Union and the State of Hungary, via the European Regional Development Fund (GINOP-2.3.2-15-2016-00009). LC has received funding from the European Research Council (ERC) under the European Union's Horizon 2020 research and innovation programme (grant agreement No. 677493 - FEVER).

Appendix A. Supplementary material

Supplementary material related to this article can be found online at https://doi.org/10.1016/j.epsl.2021.116965.

References

Annen, C., 2009. From plutons to magma chambers: thermal constraints on the accumulation of eruptible silicic magma in the upper crust. Earth Planet. Sci. Lett. 284, 409–416. https://doi.org/10.1016/j.epsl.2009.05.006.

Annen, C., Blundy, J.D., Sparks, R.S.J., 2006. The genesis of intermediate and silicic magmas in deep crustal hot zones. J. Petrol. 47, 505–539. https://doi.org/10.1093/petrology/egi084.

Bachmann, O., Oberli, F., Dungan, M.A., Meier, M., Mundil, R., Fischer, H., 2007. ^{40}Ar/^{39}Ar and U–Pb dating of the Fish Canyon magmatic system, San Juan Volcanic field, Colorado: evidence for an extended crystallization history. Chem. Geol. 236, 134–166.

Bachmann, O., Bergantz, G.W., 2006. Gas percolation in upper-crustal silicic crystal mushes as a mechanism for upward heat advection and rejuvenation of near-solidus magma bodies. J. Volcanol. Geotherm. Res. 149, 85–102.

Bindeman, I.N., 2003. Crystal sizes in evolving silicic magma chambers. Geology 31, 367–370.

Boehnke, P., Watson, E.B., Trail, D., Harrison, T.M., Schmitt, A.K., 2013. Zircon saturation re-revisited. Chem. Geol. 351, 324–334.

Burgisser, A., Bergantz, G.W., 2011. A rapid mechanism to remobilize and homogenize highly crystalline magma bodies. Nature 471, 212–215.

Caricchi, L., Blundy, J., 2015. The Temporal Evolution of Chemical and Physical Properties of Magmatic Systems. Geological Society, London. Special Publications, vol. 422, pp. 1–15.

Caricchi, L., Simpson, G., Schaltegger, U., 2014. Zircons reveal magma fluxes in the Earth's crust. Nature 511, 457–461.

Caricchi, L., Simpson, G., Schaltegger, U., 2016. Estimates of volume and magma input in crustal magmatic systems from zircon geochronology: the effect of modeling assumptions and system variables. Front. Earth Sci. 4. https://doi.org/10.3389/feart.2016.00048.

Cisneros de León, A., Schmitt, A.K., 2019. Intrusive reawakening of El Chichón volcano prior to its Holocene eruptive hyperactivity. J. Volcanol. Geotherm. Res. 377, 53–68.

Claiborne, L.L., Miller, C.F., Flanagan, D.M., Clynne, M.A., Wooden, J.L., 2010. Zircon reveals protracted magma storage and recycling beneath Mount St. Helens. Geology 38, 1011–1014.

Conway, C.E., Chamberlain, K.J., Harigane, Y., Morgan, D.J., Wilson, C.J.N., 2020. Rapid assembly of high-Mg andesites and dacites by magma mixing at a continental arc stratovolcano. Geology 48, 1033–1037. https://doi.org/10.1130/g47614.1.

Cooper, K.M., 2019. Time scales and temperatures of crystal storage in magma reservoirs: implications for magma reservoir dynamics. Philos. Trans. R. Soc. A, Math. Phys. Eng. Sci. 377, 20180009.

Cooper, K.M., Kent, A.J.R., 2014. Rapid remobilization of magmatic crystals kept in cold storage. Nature 506, 480–483.

Druitt, T.H., Costa, F., Deloule, E., Dungan, M., Scaillet, B., 2012. Decadal to monthly timescales of magma transfer and reservoir growth at a caldera volcano. Nature 482, 77–80. https://doi.org/10.1038/nature10706.

Ferry, J.M., Watson, E.B., 2007. New thermodynamic models and revised calibrations for the Ti-in-zircon and Zr-in-rutile thermometers. Contrib. Mineral. Petrol. 154, 429–437.

Folkes, C.B., de Silva, S.L., Schmitt, A.K., Cas, R.A.F., 2011. A reconnaissance of U-Pb zircon ages in the Cerro Galán system, NW Argentina: prolonged magma residence, crystal recycling, and crustal assimilation. J. Volcanol. Geotherm. Res. 206, 136–147.

Frey, H.M., Manon, M.R.F., Brehm, S.K., Babiak, R.N., 2018. Episodic crystallization in young explosive eruptions in Dominica, Lesser Antilles, revealed by U-Th dating of zircons. Geology 46, 887–890.

Friedrichs, B., Schindlbeck-Belo, J.C., Danišík, M., Jenkins, S.F., Yurteri, E., Çobankaya, M., Frische, M., Wang, K.-L., Lee, H.-Y., Atıcı, G., Schmitt, A.K., Sparks, R.S.J., 2020. New insights into source and dispersal of Mediterranean S1 tephra, an early Holocene marker horizon erupted at Mt. Erciyes (Turkey). Quat. Sci. Rev. 249, 106606. https://doi.org/10.1016/j.quascirev.2020.106606.

Friedrichs, B., Atıcı, G., Danišík, M., Yurteri, E., Schmitt, A.K., 2021. Sequence modeling in zircon double-dating of early Holocene Mt. Erciyes domes (Central Anatolia). Quat. Geochronol. 61, 101129. https://doi.org/10.1016/j.quageo.2020.101129.

Gençalioğlu-Kuşcu, G., Uslular, G., Danišík, M., Koppers, A., Miggins, D.P., Friedrichs, B., Schmitt, A.K., 2020. U–Th disequilibrium, (U–Th)/He and 40Ar/39Ar geochronology of distal Nisyros Kyra tephra deposits on Datça peninsula (SW Anatolia). Quat. Geochronol. 55, 101033. https://doi.org/10.1016/j.quageo.2019.101033.

Harangi, S., Molnár, M., Vinkler, A.P., Kiss, B., Jull, A.J.T., Leonard, A.G., 2010. Radiocarbon dating of the last volcanic eruptions of Ciomadul volcano, Southeast Carpathians, Eastern-Central Europe. Radiocarbon 52, 1498–1507. https://doi.org/10.1017/S0033822200046580.

Harangi, S., Lukács, R., Schmitt, A.K., Dunkl, I., Molnár, K., Kiss, B., Seghedi, I., Novothny, Á., Molnár, M., 2015a. Constraints on the timing of Quaternary volcanism and duration of magma residence at Ciomadul volcano, east–central Europe, from combined U–Th/He and U–Th zircon geochronology. J. Volcanol. Geotherm. Res. 301, 66–80.

Harangi, S., Novák, A., Kiss, B., Seghedi, I., Lukács, R., Szarka, L., Wesztergom, V., Metwaly, M., Gribovszki, K., 2015b. Combined magnetotelluric and petrologic constrains for the nature of the magma storage system beneath the Late Pleistocene Ciomadul volcano (SE Carpathians). J. Volcanol. Geotherm. Res. 290, 82–96.

Harangi, S., Molnár, K., Schmitt, A.K., Dunkl, I., Seghedi, I., Novothny, Á., Molnár, M., Kiss, B., Ntaflos, T., Mason, P.R.D., Lukács, R., 2020. Fingerprinting the Late Pleistocene tephras of Ciomadul volcano, eastern–central Europe. J. Quat. Sci. 35, 232–244.

Hayden, L.A., Watson, E.B., 2007. Rutile saturation in hydrous siliceous melts and its bearing on Ti-thermometry of quartz and zircon. Earth Planet. Sci. Lett. 258, 561–568.

Karakas, O., Degruyter, W., Bachmann, O., Dufek, J., 2017. Lifetime and size of shallow magma bodies controlled by crustal-scale magmatism. Nat. Geosci. 10, 446–450.

Karátson, D., Wulf, S., Veres, D., Magyari, E.K., Gertisser, R., Timar-Gabor, A., Novothny, Á., Telbisz, T., Szalai, Z., Anechitei-Deacu, V., Appelt, O., Bormann, M., Jánosi, C., Hubay, K., Schäbitz, F., 2016. The latest explosive eruptions of Ciomadul (Csomád) volcano, East Carpathians — a tephrostratigraphic approach for the 51–29ka BP time interval. J. Volcanol. Geotherm. Res. 319, 29–51.

Karátson, D., Telbisz, T., Dibacto, S., Lahitte, P., Szakács, A., Veres, D., Gertisser, R., Jánosi, C., Timár, G., 2019. Eruptive history of the Late Quaternary Ciomadul (Csomád) volcano, East Carpathians, part II: magma output rates. Bull. Volcanol. 81, 28. https://doi.org/10.1007/s00445-019-1287-8.

Kent, A.J.R., Cooper, K.M., 2017. How well do zircons record the thermal evolution of magmatic systems? Geology 46, 111–114.

Kern, J.M., de Silva, S.L., Schmitt, A.K., Kaiser, J.F., Iriarte, A.R., Economos, R., 2016. Geochronological imaging of an episodically constructed subvolcanic batholith: U-Pb in zircon chronochemistry of the Altiplano-Puna Volcanic Complex of the Central Andes. Geosphere 12, 1054–1077.

Kis, B.M., Caracausi, A., Palcsu, L., Baciu, C., Ionescu, A., Futó, I., Sciarra, A., Harangi, S., 2019. Noble gas and carbon isotope systematics at the seemingly inactive Ciomadul Volcano (Eastern-Central Europe, Romania): evidence for volcanic degassing. Geochem. Geophys. Geosyst. 20, 3019–3043.

Kiss, B., Harangi, S., Ntaflos, T., Mason, P.R.D., Pál-Molnár, E., 2014. Amphibole perspective to unravel pre-eruptive processes and conditions in volcanic plumbing systems beneath intermediate arc volcanoes: a case study from Ciomadul volcano (SE Carpathians). Contrib. Mineral. Petrol. 167, 986. https://doi.org/10.1007/s00410-014-0986-6.

Klemetti, E.W., Clynne, M.A., 2014. Localized rejuvenation of a crystal mush recorded in zircon temporal and compositional variation at the Lassen Volcanic Center, northern California. PLoS ONE 9, e113157. https://doi.org/10.1371/journal.pone.0113157.

Lahitte, P., Dibacto, S., Karátson, D., Gertisser, R., Veres, D., 2019. Eruptive history of the Late Quaternary Ciomadul (Csomád) volcano, East Carpathians, part I: timing of lava dome activity. Bull. Volcanol. 81, 27. https://doi.org/10.1007/s00445-019-1286-9.

Laumonier, M., Karakas, O., Bachmann, O., Gaillard, F., Lukács, R., Seghedi, I., Menand, T., Harangi, S., 2019. Evidence for a persistent magma reservoir with large melt content beneath an apparently extinct volcano. Earth Planet. Sci. Lett. 521, 79–90.

Lipman, P.W., Bachmann, O., 2015. Ignimbrites to batholiths: integrating perspectives from geological, geophysical, and geochronological data. Geosphere 11, 705–743.

Lukács, R., Guillong, M., Schmitt, A.K., Molnár, K., Bachmann, O., Harangi, S., 2018. LA-ICP-MS and SIMS U-Pb and U-Th zircon geochronological data of Late Pleistocene lava domes of the Ciomadul Volcanic Dome Complex (Eastern Carpathians). Data in Brief 18, 808–813.

Molnár, K., Harangi, S., Lukács, R., Dunkl, I., Schmitt, A.K., Kiss, B., Garamhegyi, T., Seghedi, I., 2018. The onset of the volcanism in the Ciomadul Volcanic Dome Complex (Eastern Carpathians): eruption chronology and magma type variation. J. Volcanol. Geotherm. Res. 354, 39–56.

Molnár, K., Lukács, R., Dunkl, I., Schmitt, A.K., Kiss, B., Seghedi, I., Szepesi, J., Harangi, S., 2019. Episodes of dormancy and eruption of the Late Pleistocene Ciomadul volcanic complex (Eastern Carpathians, Romania) constrained by zircon geochronology. J. Volcanol. Geotherm. Res. 373, 133–147.

Mori, J., Eberhard-Phillips, D., Harlow, D.H., 1996. Three-dimensional velocity structure at Mount Pinatubo: resolving magma bodies and earthquake hypocenters. In: Newhall, C.G., Punongbayan, S. (Eds.), Fire and Mud. University of Washington Press, pp. 371–385.

Patankar, S., 1980. Numerical Heat Transfer and Fluid Flow. CRC Press. 214 pp.

Popa, M., Radulian, M., Szakács, A., Seghedi, I., Zaharia, B., 2012. New seismic and tomography data in the southern part of the Harghita Mountains (Romania, Southeastern Carpathians): connection with recent volcanic activity. Pure Appl. Geophys. 169, 1557–1573.

Pritchard, M.E., Gregg, P.M., 2016. Geophysical evidence for silicic crustal melt in the continents: where, what kind, and how much? Elements 12, 121–127.

Reid, M.R., Coath, C.D., Mark Harrison, T., McKeegan, K.D., 1997. Prolonged residence times for the youngest rhyolites associated with Long Valley Caldera: ^{230}Th-^{238}U ion microprobe dating of young zircons. Earth Planet. Sci. Lett. 150, 27–39.

Reid, M.R., Vazquez, J.A., Schmitt, A.K., 2011. Zircon-scale insights into the history of a Supervolcano, Bishop Tuff, Long Valley, California, with implications for the Ti-in-zircon geothermometer. Contrib. Mineral. Petrol. 161, 293–311.

Reid, M.R., Vazquez, J.A., 2017. Fitful and protracted magma assembly leading to a giant eruption, Youngest Toba Tuff, Indonesia. Geochem. Geophys. Geosyst. 18, 156–177.

Rubatto, D., Hermann, J., 2007. Experimental zircon/melt and zircon/garnet trace element partitioning and implications for the geochronology of crustal rocks. Chem. Geol. 241, 38–61.

Rubin, A.E., Cooper, K.M., Till, C.B., Kent, A.J.R., Costa, F., Bose, M., Gravley, D., Deering, C., Cole, J., 2017. Rapid cooling and cold storage in a silicic magma reservoir recorded in individual crystals. Science 356, 1154–1156.

Sambridge, M.S., Compston, W., 1994. Mixture modeling of multi-component data sets with application to ion-probe zircon ages. Earth Planet. Sci. Lett. 128, 373–390.

Schmitt, A.K., Stockli, D.F., Lindsay, J.M., Robertson, R., Lovera, O.M., Kislitsyn, R., 2010. Episodic growth and homogenization of plutonic roots in arc volcanoes from combined U–Th and (U–Th)/He zircon dating. Earth Planet. Sci. Lett. 295, 91–103.

Seghedi, I., Szakács, A., Udrescu, C., Stoian, M., Grabari, G., 1987. Trace element geochemistry of the South Harghita volcanics (East Carpathians): calc-alkaline and shoshonitic association. Dari S. Sed. Inst. Geol. Geofiz. 72–73, 381–397.

Storm, S., Shane, P., Schmitt, A.K., Lindsay, J.M., 2011. Contrasting punctuated zircon growth in two syn-erupted rhyolite magmas from Tarawera volcano: insights to crystal diversity in magmatic systems. Earth Planet. Sci. Lett. 301, 511–520.

Szakács, A., Seghedi, I., Pécskay, Z., Mirea, V., 2015. Eruptive history of a low-frequency and low-output rate Pleistocene volcano, Ciomadul, South Harghita Mts., Romania. Bull. Volcanol. 77, 12. https://doi.org/10.1007/s00445-014-0894-7.

Szymanowski, D., Wotzlaw, J.-F., Ellis, B.S., Bachmann, O., Guillong, M., von Quadt, A., 2017. Protracted near-solidus storage and pre-eruptive rejuvenation of large magma reservoirs. Nat. Geosci. 10, 777–782.

Tierney, C.R., Schmitt, A.K., Lovera, O.M., de Silva, S.L., 2016. Voluminous plutonism during volcanic quiescence revealed by thermochemical modeling of zircon. Geology 44, 683–686.

Vazquez, J.A., Reid, M.R., 2004. Probing the accumulation history of the voluminous Toba magma. Science 305, 991–994.

Vermeesch, P., 2012. On the visualisation of detrital age distributions. Chem. Geol. 312–313, 190–194. https://doi.org/10.1016/j.chemgeo.2012.04.021.

Vinkler, A.P., Harangi, S., Ntaflos, T., Szakács, A., 2007. A Csomád vulkán (Keleti-Kárpátok) horzsaköveinek kőzettani és geokémiai vizsgálata — petrogenetikai következtetések (Petrology and geochemistry of pumices from the Ciomadul volcano (Eastern Carpathians) — implications for petrogenetic processes). Földt. Közlöny (Bull. Hung. Geol. Soc.) 137, 103–128.

Weber, G., Caricchi, L., Arce, J.L., Schmitt, A.K., 2020a. Determining the current size and state of subvolcanic magma reservoirs. Nat. Commun. 11, 5477. https://doi.org/10.1038/s41467-020-19084-2.

Weber, G., Simpson, G., Caricchi, L., 2020b. Magma diversity reflects recharge regime and thermal structure of the crust. Sci. Rep. 10, 11867. https://doi.org/10.1038/s41598-020-68610-1.

White, S.M., Crisp, J.A., Spera, F.J., 2006. Long-term volumetric eruption rates and magma budgets. Geochem. Geophys. Geosyst. 7, Q03010. https://doi.org/10.1029/2005GC001002.

Wolfe, E.W., Hoblitt, R.P., 1996. Overview of the eruptions. In: Newhall, C.G., Punongbayan, S. (Eds.), Fire and Mud. University of Washington Press, pp. 3–20.

Wotzlaw, J.-F., Schaltegger, U., Frick, D.A., Dungan, M.A., Gerdes, A., Günther, D., 2013. Tracking the evolution of large-volume silicic magma reservoirs from assembly to supereruption. Geology 41, 867–870.